https://doi.org/10.48048/tis.2022.4634

Antenna Array Miniaturization using a Defected Ground Structure

D. Shashi Kumar[*] and Sellakkutti Suganthi

RF and Microwave Research Laboratory, Department of Electronics and Communication Engineering, Christ University, Bengaluru 560074, India

([*]Corresponding author's e-mail: shashiphd2015@gmail.com)

Received: 21 February 2021, Revised: 28 June 2021, Accepted: 28 July 2021

Abstract

A novel Defected Ground Structure (DGS) is proposed to miniaturize a 2×2 Modified Corporate Feed Planar Antenna Array (M-CFPA) with a modified corporate feeding network. The DGS altered the surface current distribution and shifted the resonance frequency to the lower side. After running a parametric sweep of length and width of the patch antenna element, achieved the miniaturized antenna array resonating at 2.4 GHz frequency. The proposed antenna array is designed using Rogers/RT Duroid 5,880 ($\varepsilon_r = 2.2$) substrate with a thickness of 1.6 mm. The overall dimensions of the proposed Planar Array with DGS (PA-DGS) is 25.2723 % lesser than M-CFPA. The M-CFPA has a peak gain of 11.53 dB with a - 10 dB reflection coefficient bandwidth of 118 MHz. The proposed PA-DGS array exhibits a peak gain of 9.51 dB with 100 MHz -10 dB bandwidth.

Keywords: Miniaturized antenna, Metamaterial, Defected ground structure, Double negative material

Introduction

Antenna miniaturization has gained importance in the present wireless communication system design due to communication equipment size and portability constraints. Early research studies reported that the antenna's form-factor decrease would directly impact its bandwidth and efficiency. Many researchers started working on the antenna's miniaturization by changing the antenna's electrical and physical properties.

The most prominent miniaturization techniques are divided into 2 main categories: Material-based and topology-based [1]. The characteristics of the antenna are fully controlled by the radiation of accelerated charges in an excited antenna. Hence, by maintaining the antenna's proper current distribution and electrical dimensions, one can achieve the desired resonance and radiation characteristics by constraining the form factor (volume of the antenna array) to be as small as possible. Several methods have been reported in the past to miniaturize antennas. Some of them include introducing slots on radiating elements, high dielectric constant materials, disturbing surface current distribution using defects in the ground plane.

Several authors showed miniaturization by shifting the resonant frequency from higher frequency to lower frequency by maintaining the antenna's same physical dimensions. In their work, the resultant frequency is not specific. Hanae *et al.* [2] designed a conventional antenna resonating at 5.7 GHz and used DGS to shift the resonant frequency to 3 GHz. Rashmi *et al.* [3] presented in their work the conventional C band array and its miniaturized version resonating at S-band using a DGS, maintaining the physical volume of the antenna array constant. Avula *et al.* [4] reported a miniaturized antenna using DGS and meander structure. The conventional antenna designed in their work resonated at 15 GHz; by introducing DGS and meander structure, they achieved dual-band resonance at 7.26 and 9.42 GHz. Rebyiy *et al.* [5] showed dumbbel-shaped DGS with circular slots to shift resonant frequency from 5.8 to 2.45 GHz. Otman *et al.* [6] presented antenna array miniaturization using dumbbell DGS. The authors designed an antenna array to resonate at 10 GHz and then used DGS to shift resonant frequency to 7.5 GHz. Ahmed *et al.* [7] reported a novel dumbbell-shaped DGS with a modified patch antenna array to reduce the form-factor of the array. They showed a shifting resonant frequency from 5.8 to 2.45 GHz with the use of DGS. Ali *et al.* [8] used Rectangular Complementary Split Ring resonators (RCSRR) to demonstrate the antenna's miniaturization and achieved about 46.8 %. Shashi *et al.* [9] reported an antenna array with metamaterial superstrate. They showed the improved radiation characteristics at the

cost of increased form factor. Nosrati *et al.* [10] presented a circularly polarized antenna array with metasurface. Prakasam *et al.* [11] showed the design of a circular microstrip patch antenna array. Ayn *et al.* [12] demonstrated the effect of air-gap in their 2×2 antenna array. Farooq *et al.* [13] presented a 1×4 antenna array with a Coplanar Waveguide (CPW) feeding mechanism. Attia *et al.* [14] used magnetic superstrates with the antenna array to improve the radiation characteristics.

In this article, the authors proposed an array of metamaterial as DGS. This method is adopted to miniaturize a 2×2 modified corporate feed array. Initially, the authors designed the antenna array to resonate at 2.4 GHz. The ground plane defect is introduced by using a unique combination of DGS unit cells. The defect introduced in the ground plane changed the current distribution and shifted the resonant frequency from 2.4 to 2.242 GHz, not the desired resonant frequency, which is one of the objectives of the proposed work. Hence authors carried out a parametric analysis to adjust the dimensions after introducing the DGS to get a miniaturized antenna array resonating at the desired 2.4 GHz frequency. The overall dimensions of the 2×2 array is reduced to $0.937\lambda_o x 0.824\lambda_o$ from $1.02\lambda_o x 0.969\lambda_o$, which is almost 25.2723 %. The novelty in this work is in: (a) the design of a Double Negative (DNG) metamaterial array and its effective use in miniaturization of the antenna array.

Materials and methods

To study the performance of the antenna array designed, simulations are carried out using computational electromagnetic solver HFSS Ver. 18.2. The geometry of the M-CFPA and the defected ground plane used for miniaturization of M-CFPA is shown in **Figure 1**. The optimum dimensions of the designed M-CFPA antenna array are presented in **Table 1**.

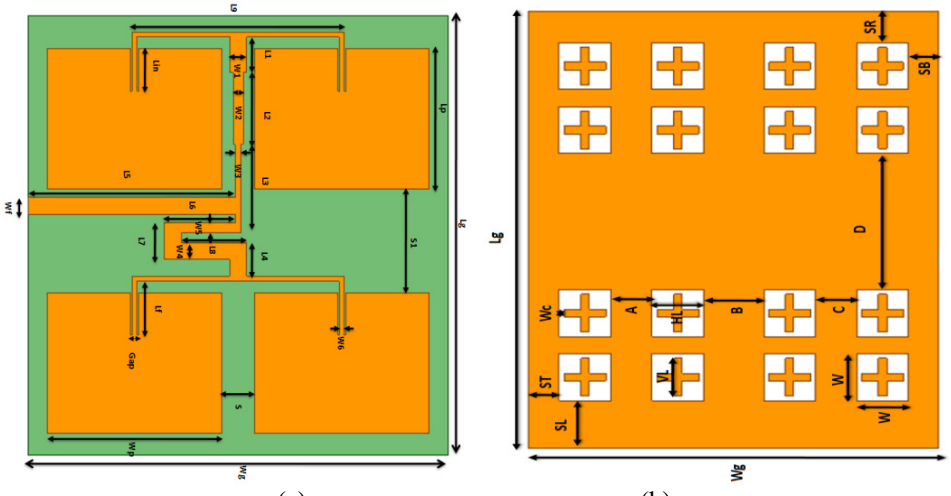

(a) (b)

Figure 1 (a) Geometry of M-CFPA and (b) geometry of defected ground plane.

After a detailed parametric study, the optimum dimensions obtained for the PA-DGS are presented in **Table 2**. The slot's width and the arm length of the metallic plus symbol used in the unit cell are parameterized to study the effect and fixed the dimensions as W = 12.5 mm and VL = HL = 10 mm. Then, the patch's length and width are parameterized to get the optimum patch length and width as 35.968 mm and 39.712 mm, respectively.

Table1 Optimum dimensions of M-CFPA.

Parameter	Value in mm	Parameter	Value(mm)	Parameter	Value (mm)
Lg	127.096	L1	10.337	W1	4.93
Wg	121.086	L2	20.674	W2	2.866
Lp	40.65	L3	25.501	W3	1.404

Parameter	Value in mm	Parameter	Value(mm)	Parameter	Value (mm)
Wp	50.24	L4	9.729	W4	4.93
Lf	15.668	L5	59.84	W5	2.866
Wf	4.93	L6	20.674	W6	1.404
Lin	12.272	L7	10.662		
Gap	2.399	L8	18.911		
S	42.137	L9	61.245		

Table 2 Optimum dimensions of PA-DGS.

Parameter	Value in mm	Parameter	Value (mm)	Parameter	Value (mm)
Lg	116.607	L1	10.337	W1	4.93
Wg	98.624	L2	20.674	W2	2.866
Lp	35.968	L3	20.8191	W3	1.404
Wp	39.712	L4	9.729	W4	4.93
Lf	16.79	L5	48.61	W5	2.866
Wf	4.93	L6	20.674	W6	1.404
Lin	13.4	L7	10.662	S1	29.8625
Gap	2.399	L8	18.911		
S	9.6	L9	50.716		

The final dimensions of the defected ground plane used in the array miniaturization are tabulated in **Table 3**. To verify the double negative behaviour of the unit cell (used as a DGS in PA-DGS), simulation were carried out using HFSS software. The model of metamaterial unit cell simulated is shown in **Figure 2**. In this model, a waveguide with orthogonal electric and magnetic boundaries is used with waveguide ports labelled as 1 and 2 as input and out ports.

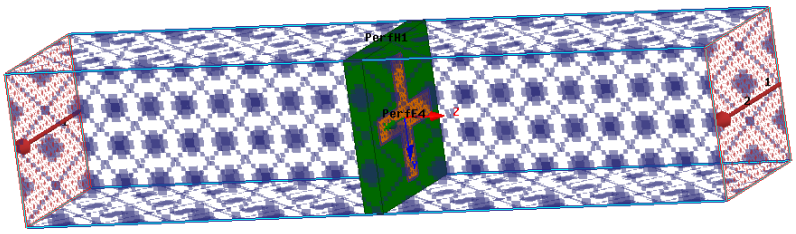

Figure 2 Simulation model of metamaterial unit cell used as DGS in PA-DGS.

Table 3 Optimum dimensions of defected ground plane.

Parameter	Value in mm	Parameter	Value (mm)
Lg	116.607	VL	10
Wg	98.624	HL	10
SL	5.508	Wc	2
SR	4.8	A	9.912
ST	4.8	B	14.4
SB	4.8	C	9.912
W	12.5	D	36.2625

The non-symmetric modified corporate feed network used in the antenna array design is presented in **Figure 3**. In this design, the elements of the antenna array are excited with uniform current distribution. The impedance of each segment used in the feed network are given in **Figure 3**. The source is connected to a 50 Ω feed then it is split into two 100 Ω branches to divide source power equally in the initial stage. Then the 100 Ω lines are transformed into 50 Ω lines by using a quarter-wave transformer of 70.7 Ω. In the final step, again, the 50 Ω lines are split into two 100 Ω lines to match the impedance of antenna elements for maximum power transfer.

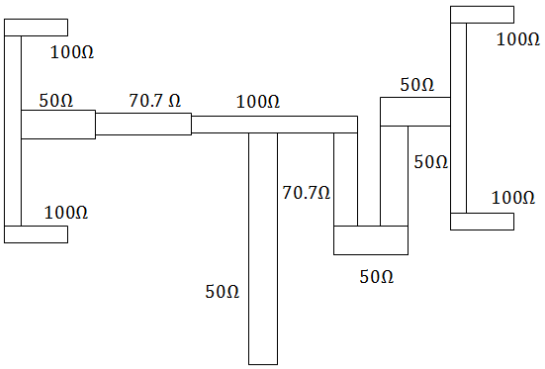

Figure 3 Modified corporate feed network.

Experimental setup and characterization

To validate the simulation results, Anritsu S820E Vector Network analyzer is used and measurements were carried out. **Figures 4(a)** and **(b)** are the snapshots of the reflection coefficient measurement. **Figure 4(c)** shows the measured impedance, and **Figure 4(d)** depicts the measurement of VSWR for the proposed PA-DGS antenna array. All measured results are in good agreement with the simulation results.

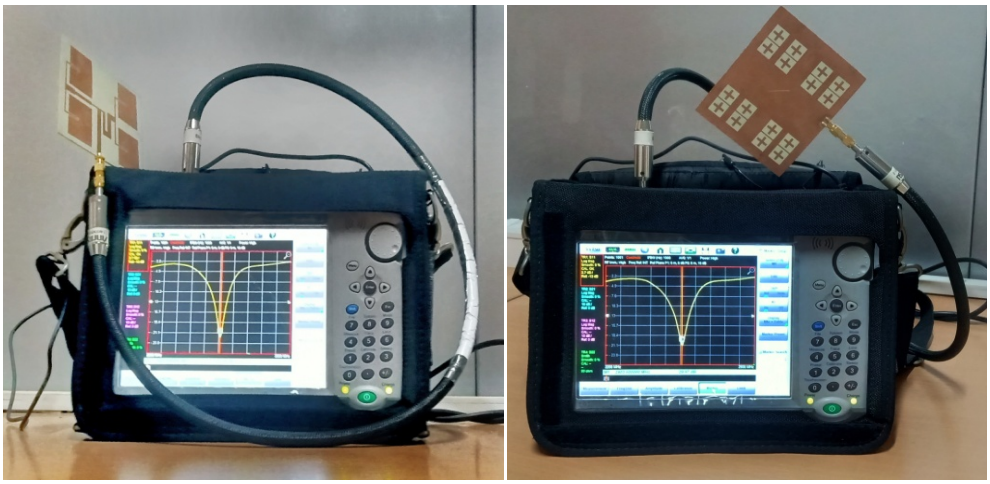

(a) (b)

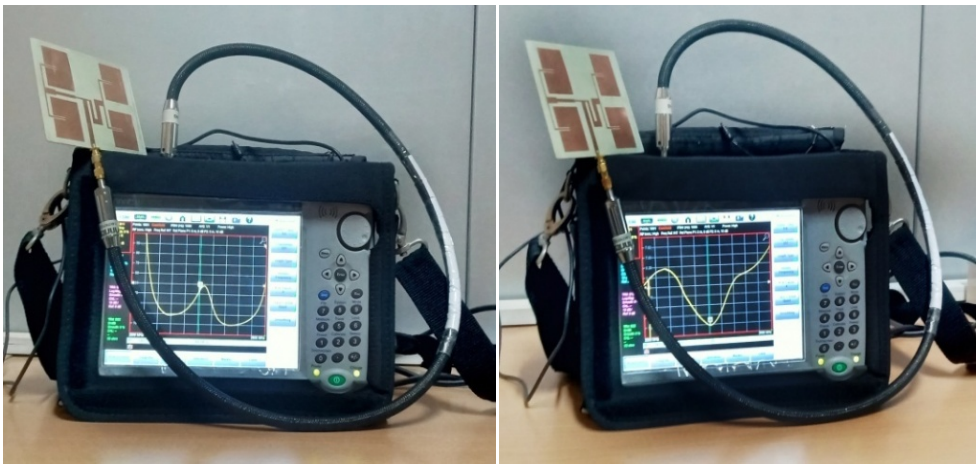

(c) (d)

Figure 4 (a) and (b) Measurement of reflection coefficient (c) measurement of impedance (d) measurement of VSWR.

Results and discussion

The simulation results of the metamaterial unit cell are presented in **Figure 5**. From the traces, one can observe that the unit cell exhibits the negative permittivity and permeability between 1 to 7.2 GHz, resulting in a negative refractive index between 1 to 7.2 GHz. The simulation results confirm that the unit cell used as a DGS is a metamaterial.

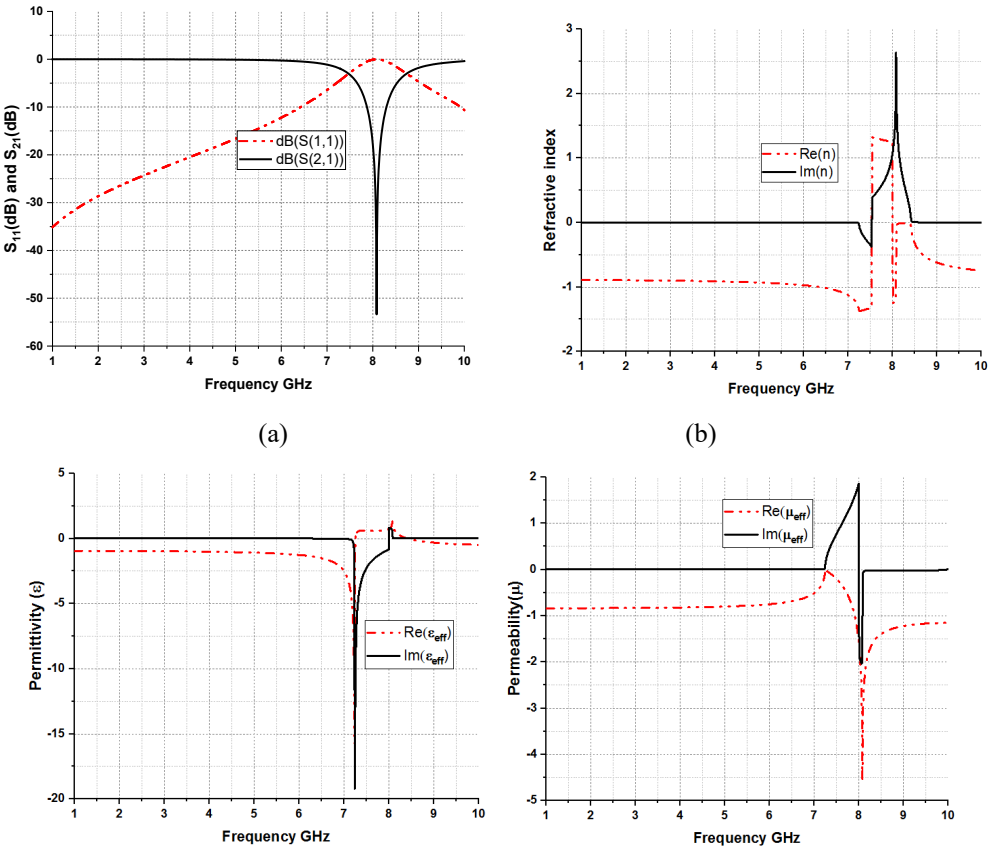

(a) (b)

(c) (d)

Figure 5 The permittivity, permeability and refractive index of the unit cell.

Figure 6 shows the unit cell's optimization results. From these results, one can infer that the selection of appropriate dimensions and the placement of DGS greatly influence the resonance and radiation characteristics of the antenna. Among all variants, the dark black line of W = 12.5 mm in **Figure 6(a)** and the dark black line of HL = VL = 5 mm in **Figure 6(b)** shows a perfect resonance at 2.4 GHz with a reflection coefficient of −33.15 dB.

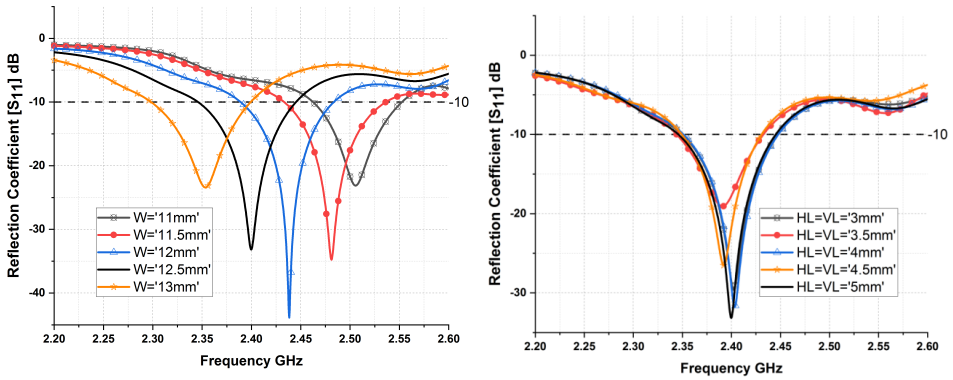

(a) (b)

Figure 6 Parametric results of DGS unit cell.

The parametric analysis results of patch length and width optimization of PA-DGS are depicted in **Figure 7**. The traces in **Figures 7(a)** and **(b)** confirms that using Lp = 35.968 mm and Wp = 39.712 mm will yield the desired resonant frequency of 2.4 GHz with a reflection coefficient of −33.15 dB.

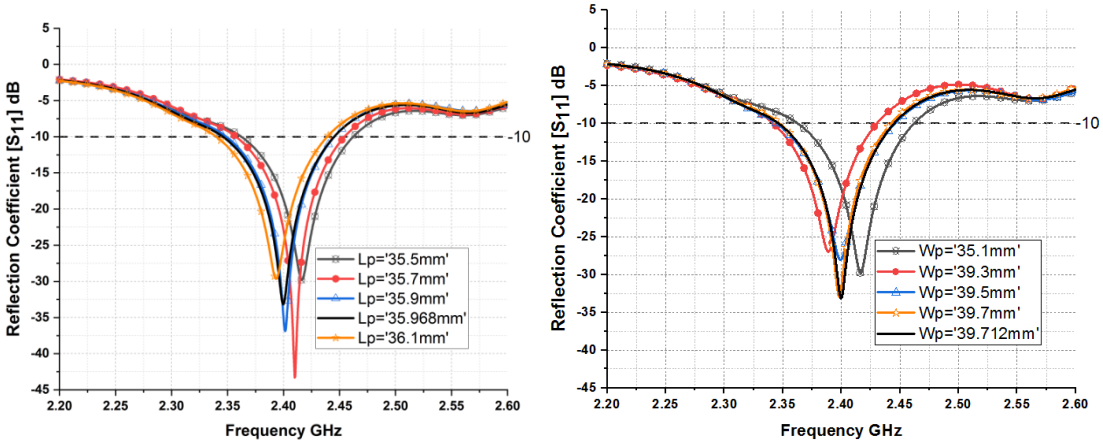

(a) (b)

Figure 7 Parametric results of patch dimensions (a) Length of the patch (b) Width of the patch

The comparison of M-CFPA and PA-DGS reflection coefficients are plotted in **Figure 8(a)**. The traces show that the M-CFPA has a - 10 dB bandwidth of 118 MHz, and the PA-DGS exhibits 100 MHz. One can also infer an excellent impedance matching at 2.4 GHz in PA-DGS as its reflection coefficient is much smaller than M-CFPA.

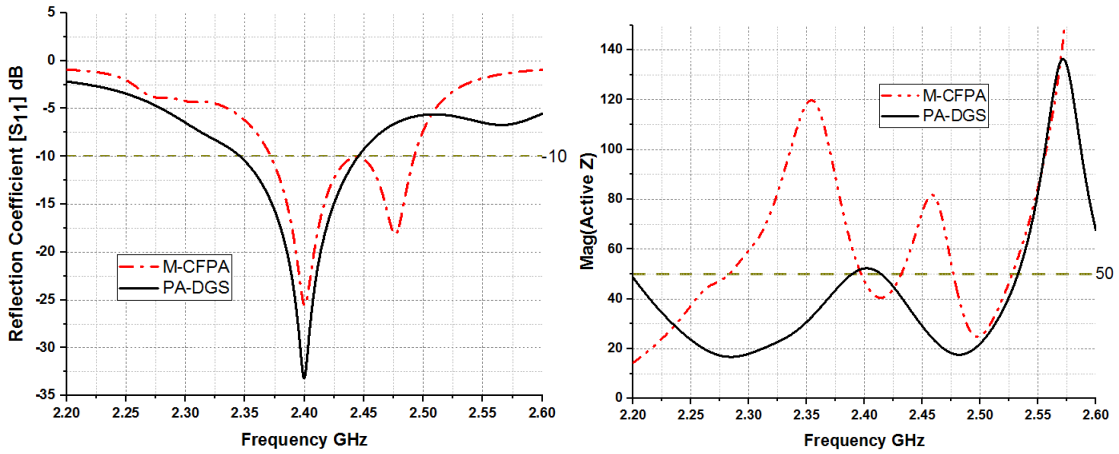

(a) (b)

Figure 8 (a) Comparison of reflection coefficient (b) comparison of impedance matching.

Figure 8(b) presents the M-CFPA and PA- DGS impedance matching throughout the frequency range. From the traces, one can infer both antenna arrays exhibit excellent impedance matching at 2.4 GHz. The plotted results confirm that the dimensions are very well optimized to get better resonance characteristics.

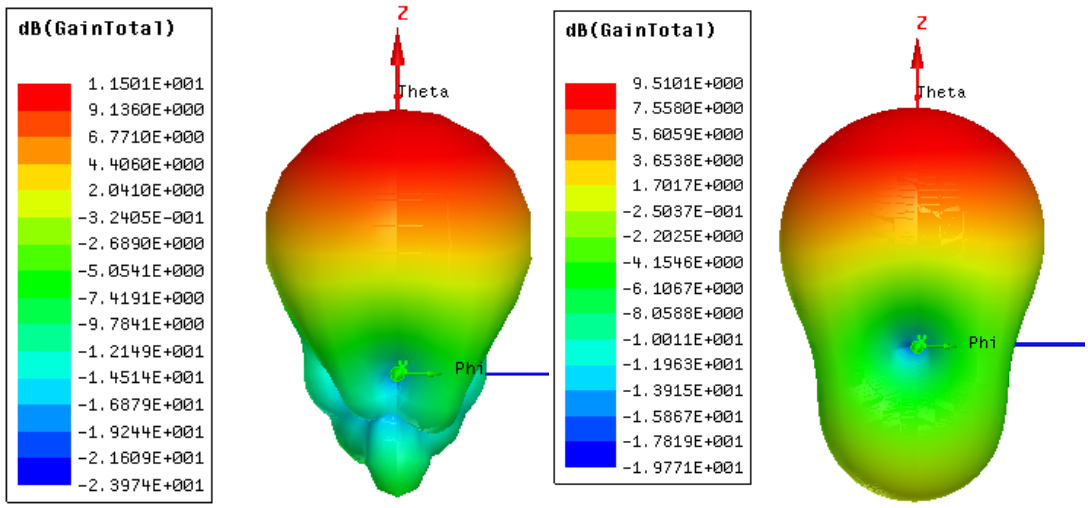

(a) (b)

Figure 9 3D radiation patterns (a) M-CFPA (b) PA-DGS.

Figure 9 depicts the radiation behaviour of M-CFPA and PA-DGS. The 3D radiation patterns of M-CFPA and PA-DGS shows directive radiation patterns at 2.4 GHz. The major lobe of the radiation pattern is at $\theta = 0^0$. The maximum gain exhibited by M-CFPA and PA - DGS are 11.5 dB and 9.51 dB, respectively. The decrease in gain in PA-DGS is directly related to the form-factor of the antenna array. Due to miniaturization, a slight reduction in gain is observed.

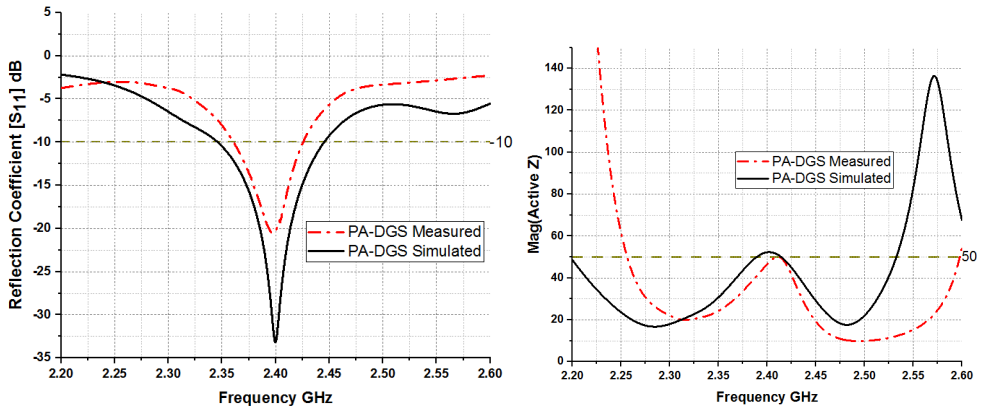

(a) (b)

Figure 10 (a) Comparison of simulated and measured reflection coefficient (b) comparison of simulated and measured impedance.

The compassion of simulated and measured reflection coefficient and magnitude of impedance for PA-DGS are presented in **Figures 10(a)** and **(b)**, respectively. From the traces, one can notice that the simulated and measured results have good agreement with each other. The minor variations in the results are due to the imperfections in fabrication, soldering of the connector and experimental environment.

Conclusions

A novel DGS unit cell configuration is used to miniaturize the M-CFPA. The contrast between M-CFPA and PA-DGS are presented in **Table 4**. From the tabulated results, it is clear that antenna arrays miniaturization will slightly degrade its radiation performance. But due to parametric optimization, an excellent impedance matching is achieved with a reflection coefficient of −33.15 dB at the desired resonant frequency of 2.4 GHz. PA-DGS has a form-factor 25.2723 % lesser than M-CFPA; the miniaturization of the antenna array is confirmed due to DGS use. Since both the antenna arrays presented in this paper exhibit good resonance radiation characteristics at 2.4 GHz ISM band frequency, we can use them in WLAN applications where directive beams with high gain are required.

Table 4 Contrast between M-CFPA and PA-DGS.

Parameter	M-CFPA	PA-DGS
Gain (dB)	11.53	9.51
RL (dB)	-25.55	-33.15
BW (MHz)	118	100
VSWR	1.11	1.045
Z (Ohm)	46.95	52.249
Size	$1.02\lambda_o$x$0.969\lambda_o$	$0.933\lambda_o$x$0.789\lambda_o$

Table 5 presents the comparison of proposed PA-DGS with the similar designs available in the literature. The table shows that the proposed PA-DGS exhibits a smaller overall size compared to all antenna arrays reported in the literature covered.

Table 5 Comparison of proposed antenna array with designs available in literature.

Ref	Permittivity ϵ_r	Frequency $f_r(GHz)$	$S_{11}(dB)$	Gain (dB)	Size (mm)
Proposed	2.2	2.4	−33.15	9.51	$0.933\lambda_o \times 0.789\lambda_o$
[9]	4.4	2.4	−11.7	9.46	$1.94\lambda_0 \times 0.48\lambda_0$
[10]	4.4	2.4	−11.25	8.6	$1.90\lambda_0 \times 1.90\lambda_0$
[11]	2.45	2.45	−40.115	12.406	$2.86\lambda_0 \times 0.8\lambda_0$
[12]	4.4	2.4	−15.194	6.47	$0.54\lambda_0 \times 1.93$
[13]	4.4	2.4	−22.87	8.25	$2.7\lambda_0 \times 0.72\lambda_0$
[14]	4.4	2.4	−22.87	8.25	$2.7\lambda_0 \times 0.72\lambda_0$

Acknowledgements

The authors are thankful to the CHRIST (Deemed to be University) for facilitating the state of the art research laboratory to carry out simulation studies and experimental validation of the proposed design.

References

[1] M Fallahpour and R Zoughi. Antenna miniaturization techniques: A review of topology and material based methods. *IEEE Antenn. Propag. Mag*. 2018; **60**, 38-50.

[2] H Elftouh, NA Touhami, M Aghoutane, SE Amrani, A Tazón and M Boussouis. Miniaturized microstrip patch antenna with defected ground structure. *Progr. Electromagn. Res. C* 2014; **55**, 25-33.

[3] RA Pandhare, Pl Zade and MP Abengaonkar. Miniaturized microstrip antenna array using defected ground structure with enhanced performance. *Eng. Sci. Tech. Int. J.* 2016; **19**, 1360-7.

[4] A Swetha and KR Naidu. Miniaturized antenna using DGS and meander structure for dual-band application. *Microw. Opt. Tech. Lett.* 2020; **62**, 3556-63.

[5] RE Rebyiy, J Zbitou, M Latrach, A Tajmouati, A Errkik and LE Abdellaoui. New miniature planar microstrip antenna using DGS for ISM applications. *Telkomnika* 2017; **15**, 1149-54.

[6] O Oulhaj, NA Touhami, M Aghoutane and A Tazon. A miniature microstrip patch antenna array with defected ground structure. *Int. J. Microw. Opt. Tech.* 2016; **11**, 32-9.

[7] A Ghaloua, J Zbitou, LE Abdellaoui, A Errkik, A Tajmouati and M Latrach. A miniature circular patch antenna using defected ground structure for ism band applications. *In*: Proceedings of the 2nd International Conference on Computing and Wireless Communication Systems, Larache, Morocco. 2017.

[8] T Ali, AWM Saadh, RC Biradar, J Anguera and A Andújar. A miniaturized metamaterial slot antenna for wireless applications. *AEU Int. J. Electron. Comm.* 2017; **82**, 368-82.

[9] DS Kumar and S Suganthi. Antenna array with non-uniform excitation and DNG hybrid metasurface for next generation communication equipment. *Int. J. Microw. Opt. Tech.* 2021; **16**, 175-83.

[10] M Nosrati, C Yang, X Liu and N Tavassolian. Wideband circularly polarized, slot antenna array loaded with metasurface. *Microw. Opt. Tech. Lett.* 2020; **62**, 2976-88.

[11] V Prakasam and P Sandeep. Design and analysis of 2×2 circular micro-strip patch antenna array for 2.4 GHz wireless communication application. *Int. J. Innovat. Eng. Manag. Res.* 2018; **7**, 101-08.

[12] Q Ayn, PAN Rao, PM Rao and BS Prasad. Design and analysis of high gain 2×2 and 2×4 circular patch antenna arrays with and without air-gap for WLAN applications. *In*: 2018 Conference on Signal Processing and Communication Engineering Systems, Vijayawada, India. 2018.

[13] U Farooq, A Iftikhar, A Fida, MS Khan, MF Shafique, SM Asif and RM Shubair. Design of a 1×4 CPW microstrip antenna array on PET substrate for biomedical applications. *In*: Proceedings of the 2019 IEEE International Symposium on Antennas and Propagation and USNC-URSI Radio Science Meeting, Georgia, United States. 2019.

[14] H Attia, L Yousefi, MM BaitSuwailam, MS Boybay and OM Ramahi. Enhanced-gain microstrip antenna using engineered magnetic superstrates. *IEEE Antenn. Wireless. Propag. Lett.* 2009; **8**, 1198-201.